Am J Physiol Lung Cell Mol Physiol 298: L335–L347, 2010.
First published December 18, 2009; doi:10.1152/ajplung.00190.2009.

Functional importance of the NH_2-terminal insertion sequence of lung surfactant protein B

Shelli L. Frey,[1]* Luka Pocivavsek,[1]* Alan J. Waring,[2–4] Frans J. Walther,[2,5] Jose M. Hernandez-Juviel,[2] Piotr Ruchala,[3] and Ka Yee C. Lee[1]

[1]*Department of Chemistry, Institute for Biophysical Dynamics and James Franck Institute, The University of Chicago, Chicago, Illinois;* [2]*Los Angeles Biomedical Research Institute at Harbor-UCLA Medical Center; Departments of* [3]*Medicine and* [4]*Pediatrics, UCLA School of Medicine, Los Angeles, California; and* [5]*Department of Pediatrics, Leiden University Medical Center, Leiden, The Netherlands*

Submitted 4 June 2009; accepted in final form 17 December 2009

Frey SL, Pocivavsek L, Waring AJ, Walther FJ, Hernandez-Juviel JM, Ruchala P, Lee KY. Functional importance of the NH_2-terminal insertion sequence of lung surfactant protein B. *Am J Physiol Lung Cell Mol Physiol* 298: L335–L347, 2010. First published December 18, 2009; doi:10.1152/ajplung.00190.2009.—Lung surfactant protein B (SP-B) is required for proper surface activity of pulmonary surfactant. In model lung surfactant lipid systems composed of saturated and unsaturated lipids, the unsaturated lipids are removed from the film at high compression. It is thought that SP-B helps anchor these lipids closely to the monolayer in three-dimensional cylindrical structures termed "nanosilos" seen by atomic force microscopy imaging of deposited monolayers at high surface pressures. Here we explore the role of the SP-B NH_2 terminus in the formation and stability of these cylindrical structures, specifically the distribution of lipid stack height, width, and density with four SP-B truncation peptides: SP-B 1–25, SP-B 9–25, SP-B 11–25, and SP-B 1–25Nflex (prolines 2 and 4 substituted with alanine). The first nine amino acids, termed the insertion sequence and the interface seeking tryptophan residue 9, are shown to stabilize the formation of nanosilos while an increase in the insertion sequence flexibility (SP-B 1–25Nflex) may improve peptide functionality. This provides a functional understanding of the insertion sequence beyond anchoring the protein to the two-dimensional membrane lining the lung, as it also stabilizes formation of nanosilos, creating reversible repositories for fluid lipids at high compression. In lavaged, surfactant-deficient rats, instillation of a mixture of SP-B 1–25 (as a monomer or dimer) and synthetic lung lavage lipids quickly improved oxygenation and dynamic compliance, whereas SP-B 11–25 surfactants showed oxygenation and dynamic compliance values similar to that of lipids alone, demonstrating a positive correlation between formation of stable, but reversible, nanosilos and in vivo efficacy.

lipid monolayer; atomic force microscopy; nanosilo

PULMONARY SURFACTANT is a complex mixture of phospholipids and proteins synthesized, stored, and secreted by alveolar type II cells that is essential for facilitating the respiratory mechanics of the mammalian lung (5, 29). The lack, deficiency, or inactivation of this essential material due to immaturity of type II pneumocytes in premature infants or various diseases in adults can result in respiratory distress syndrome (RDS; Refs. 2, 55). Treatment of neonatal respiratory distress syndrome (NRDS) is simplified by the lack of underlying pathology (36). The neonatal lungs need only to be stabilized for a given amount of time until type II cells mature and begin producing surfactant. Typical surfactant replacement therapies for neonates use exogenous surfactants from animal sources (51). While such therapies are costly and carry the risk of immune response, the short duration of neonate therapy minimizes the risks and makes them effective therapeutics for NRDS (13). Treatment of acute RDS (ARDS) is complicated by pathological processes that are the initial culprits of respiratory distress (45). One consequence of this is that surfactant replacement therapy is necessary for longer periods of time until the underlying systemic pathology is resolved and the lungs are healed. Another important difference is the total lung size since adult lung volumes are more than an order of magnitude larger than neonatal lungs (61). This necessitates a much larger dose of replacement surfactants, which, when combined with longer treatment times in adults, makes the development of a cost-effective synthetic surfactant replacement therapy paramount to battling ARDS.

Native lung surfactant consists of ~90% lipid and 10% protein by mass. The lipid components, mainly dipalmitoylphosphatidylcholine (DPPC) (33) and phosphatidylglycerol (PG), reduce surface tension at the air/liquid interface in the lung and prevent alveolar collapse at end expiration. It has been demonstrated that nebulized DPPC alone does not work as a surfactant therapy (60). The lipid components alone are not as effective as a biologically active lung surfactant (1, 28), but can be successfully augmented by a comparatively small in concentration, but crucially important, protein component of the surfactant. There are at least four surfactant proteins, designated as SP (surfactant protein)-A, SP-B, SP-C, and SP-D (29, 30). SP-A and SP-D are relatively large carbohydrate binding hydrophilic glycoproteins that are thought to play an instrumental role in the immune system (25). Knockout mice engineered with deactivated SP-A or SP-D expression have significantly higher susceptibility to infection compared with wild-type animals, but suffer no apparent respiratory dysfunction (43). SP-B and SP-C are smaller surfactant-associated hydrophobic proteins directly interspersed into the lipid component of the surfactant, which generate and maintain the surface-active monolayer film (29, 30). SP-C is proposed to maintain association of lipid-protein complexes with the interfacial film at the most compressed states achieved at the end of exhalation (56). In animal models, knockout of the SP-C gene results in the development of chronic respiratory diseases due to instability in the alveolar space (20). SP-B deficiency causes the most severe surfactant dysfunction, ranging from interruption of tubular myelin formation to discharge of disrupted

* S. L. Frey and L. Pocivavsek contributed equally to this work.

Address for reprint requests and other correspondence: K. Y. Lee, Univ. of Chicago, 929 E. 57th St., GCIS 139B, Chicago, IL 60637 (e-mail: kayeelee@uchicago.edu).

lamellar bodies into the airway and results in lethal pulmonary compromise in humans and animal models, indicating that this peptide performs a function absolutely indispensable for normal breathing (10, 27, 34, 47, 64). Therefore, SP-B, or a functional peptide analog of the protein, is an important component of a synthetic surfactant therapy for RDS (51). An understanding of how the protein structure dictates function is necessary to define minimal structural constructs of a synthetic peptide able to mimic SP-B functions in vitro and in vivo that is also simpler to engineer and manufacture than the native SP-B recombinant protein.

SP-B is a 79-residue, lipid associating protein found in mammalian lung surfactant at a concentration of ~1 wt% and is considered to be a member of the saposins, a family of proteins that interact with lipids, have a primarily α-helical secondary structure and share intramolecular disulfide bond patterns (47). Although much work has been done on the structure and the activity of SP-B (9, 15, 66), its specific interactions and molecular orientations in interfacial phospholipid films at different points of compression and expansion are not yet completely defined. Because synthesizing a proper folding mimic of this 79-residue protein is difficult, various shorter peptide models have been developed and characterized both structurally and functionally, among them, an NH_2-terminal truncation peptide, SP-B 1–25. Studies have shown that this SP-B analog has surface-active behavior similar to that of the full-length protein and could potentially be incorporated into synthetic surfactant formulations (23, 24, 40, 41). This NH_2-terminal sequence has been shown to interact specifically with fluid phase palmitoyloleoylphosphatidylglycerol (POPG) in mixed monolayers, similar to native SP-B, and leads to morphologies as seen in Survanta (a bovine lung surfactant replacement therapy) monolayers that contain native SP-B (15).

While there are no high-resolution crystal or NMR structures of the native SP-B protein, the structure of the NH_2 terminus up to residue 25 is well defined as determined by a combination of NMR, FTIR, and Raman spectroscopy (6, 22, 38, 53, 59, 71). Residues 1–9 (FPIPLPYCW), proposed to act as an "insertion sequence," comprise a hydrophobic region containing a poly-proline-like sequence. This region also contains a tryptophan residue at position 9 thought to help anchor the peptide at the fluid/lipid interface (12, 72). The remainder of the sequence, residues 10–25 (LCRALIKRIQAMPIAMIPKG), is an amphipathic helix with the hydrophilic side lined with four cationic residues and the hydrophobic side dominated by alanine, leucine, and isoleucine residues (38). The functional effect of structural motifs found in SP-B 1–25 has been tested by the synthesis of peptoids based on this general design with a hydrophobic, helical insertion region with aromatic side chains, which show comparable biomimetic surface activity to SP-B 1–25 (58).

The key mechanical functions of the multi-component pulmonary surfactant lining the alveolar spaces are reducing the work of breathing by lowering the surface tension at the alveolar/air interface and mechanically stabilizing the alveolar branches as well as the distribution of alveolar sizes, preventing atelectasis (48). In this work, we focus on the surface tension lowering function of lung surfactant. Human lungs are dynamic with alveolar surface area changing and alveolar surface tension fluctuating from 20 mN/m during a deep inhalation to <9 mN/m on deep exhalation (54). In vitro experiments using lipid monolayers in Langmuir trough geometries have shown that while lung surfactant films are capable of reaching low surface tensions, they begin to lose their flat interfacial geometry (40). This movement of surfactant from a two-dimensional to a three-dimensional space is termed collapse. It is hypothesized that for lung surfactant to function properly, its mode of collapse must be reversible. Thus the transfer of surface-active material from the aqueous region close to the interface followed by interfacial adsorption of the surface-active molecules to form the monolayer film must occur both postcollapse on inhalation and when newly synthesized surfactant is spread to the surface. The mixture of lipids and proteins previously discussed has been evolutionarily optimized in pulmonary surfactant to exhibit simultaneously the ability to lower air/water surface tension to nearly zero while maintaining interfacial integrity and reversibility. Designing an artificial surfactant must take these criteria into account.

The multi-function capacity of lung surfactant presents an interesting problem from the design point of view because based on pure component phase behavior, individual lipids can be classified as those capable of maintaining low surface tension or those that fluidize and help with adsorption and reversibility, but the properties are mutually exclusive (42, 44). Lipids that can achieve low surface tensions, such as the saturated lipid DPPC, adsorb poorly from solution and become rigid and brittle at low surface tensions, often collapsing via cracking and resulting in poor film respreadability. Such behavior is undesirable for proper surfactant function because the monolayer would need to be replenished after each breathing cycle. Conversely, lipids that fluidize the layer, such as unsaturated POPG, cannot achieve low surface tension. In reality, the lung surfactant monolayer is a composite material of DPPC mixed with more fluid, unsaturated lipids like POPG. The DPPC condensed domains become embedded in a softer lipid matrix composed primarily of POPG and this composite sheet has a more elastic response with good respreadability. However, it is known from studies of binary lipid mixtures that some of the POPG is selectively removed or "squeezed-out" from the monolayer above its collapse pressure of 48 mN/m (63). It has therefore been postulated that one of the main functions of SP-B is to help fluid lipid components maintain association with the surface at high compressions beyond the intrinsic collapse pressure of these lipids. Thus, when the surface pressure is reduced on expansion, the lipids can be reincorporated into the monolayer at the interface, recreating the fully composite monolayer.

Various experimental methods have explored how SP-B helps keep fluid lipids anchored to the monolayer (14, 15, 37) in the form of three-dimensional reservoirs (termed "nanosilos") of lipids and proteins in the subphase. Work with the full-length SP-B protein has shown the existence of nanosilos protruding from the anionic PG-rich areas of the monolayer (37), while experiments with the dimeric form of SP-B 1–25 have demonstrated unequivocally that both the peptide and biologically relevant anionic PG lipids were needed to form the reservoirs (15). In the present work, we further explore the role of the SP-B NH_2-terminal insertion sequence in model surfactant membranes and animal models. In model membranes of 7:3 DPPC:POPG, different truncation SP-B peptides (SP-B 1–25, SP-B 9–25, SP-B 11–25, and SP-B 1–25Nflex) were characterized in terms of their ability to form stable, reversible

nanosilos when compressed to high surface pressures; this was further compared with in vivo efficacy as a lung surfactant replacement. Nanosilos are formed by monomeric SP-B 1–25, but their integrity is compromised by the deletion of the NH_2-terminal insertion sequence while increased flexibility of this region appears to enhance the efficacy of nanosilo formation. To model the viscosity of alveolar lining fluid, parallel experiments were run on a glycerol subphase and nanosilo formation was shown to be hindered by the viscous subphase. These data combined with results from animal studies indicate that NH_2-terminal SP-B truncation peptides containing the insertion sequence promote the formation of tall, large nanosilos, which correlates with increased efficacy of the surfactant in vivo.

MATERIALS AND METHODS

Materials. Peptide synthesis reagents were purchased from AnaSpec (San Jose, CA), HPLC solvents from Fisher (Pittsburgh, PA), and all other chemicals from Sigma (St. Louis, MO) and Aldrich (Milwaukee, WI). Palmitic acid, dipalmitoylphosphatidylcholine (DPPC), dioleoylphosphatidylcholine (DOPC), palmitoyloleoylphosphatidylglycerol (POPG), palmitoyloleoylphosphatidylethanolamine (POPE), palmitoyloleoylphosphatidylserine (POPS), and cholesterol were obtained in powder form from Avanti Polar Lipids, (Alabaster, AL) and used without further purification. Adult male Sprague-Dawley rats, weighing 200 to 225 g were obtained from Harlan (San Diego, CA).

For all Langmuir trough experiments, the fluorescent probe used for visualization with fluorescence microscopy was Texas Red-labeled 1,2-dihexadecanoyl-*sn*-glycerol-3-phosphoethanolamine (TR-DHPE; Molecular Probes, Eugene, OR). The subphase was ultra-pure water (resistivity $\geq$18 MΩcm) processed by a Milli-Q ultrapurification system (A-10 gradient, Millipore, Bedford, MA) or 40 wt% glycerol (Sigma-Aldrich). Since experiments were performed on monolayers containing POPG, ultra high purity Argon 5.0 (Airgas) was used to minimize oxidative damage to the unsaturated oleoyl chain.

Synthesis of SP-B peptides. SP-B peptides were synthesized using Fmoc chemistry with a CEM Liberty microwave peptide synthesizer (Matthews, NC) and purified by reverse phase HPLC. The sequences of monomeric SP-B 1–25, SP-B 9–25, and SP-B 11–25 were based on the NH_2 terminus of human SP-B with one variation—cysteine 11 was replaced with alanine (a C11A variant monomer)—to prevent possible dimerization. SP-B 1–25Nflex is a variant of SP-B 1–25 with prolines 2 and 4 replaced with alanine (P2,4A). Dimeric SP-B 1–25 and SP-B 11–25 were formed by oxidizing the native sequence of monomeric SP-B 1–25 and SP-B 11–25 to form a disulfide linkage between the cysteine 11 residues. Porcine SP-B was isolated from porcine lung surfactant (54) and purity checked by HPLC and MALDI mass spectrometry. Porcine SP-B was used as a positive control for synthetic SP-B peptides.

Langmuir trough. Details of the Langmuir trough setup have been discussed previously (17, 21). Briefly, the setup consisted of a custom-made Teflon trough equipped with two Teflon barriers whose motions were precisely controlled by a pair of translational stages (UTM100, Newport, Irvine, CA) for symmetric compression or expansion of monolayers at the gas/water interface. A stationary Wilhelmy balance (Riegler and Kirstein, Berlin, Germany) was used to measure surface pressure. As the surface area is reduced (compression) or increased (expansion), the change in surface pressure was monitored, giving rise to surface pressure (Π) vs. area (A) isotherms. Subphase temperature was maintained within 0.5°C of the desired temperature of 25°C with a homebuilt control station comprised of thermoelectric units (Marlow Industries, Dallas, TX) joined to a heat sink held at 20°C by a Neslab RTE-100 water circulator (Portsmouth, NH). A piece of resistively heated coverglass (Delta Technologies, Dallas, TX) was placed over the trough and held at a temperature to suppress evaporative losses, minimize convective currents, and prevent condensation of water on the microscope objective.

The trough assembly was fixed to a custom-built microscope stage to allow simultaneous fluorescence microscopy with a $\times$50 extra-long working distance objective (Nikon Y-FL, Fryer, Huntley, IL). A high-pressure mercury lamp (Osram Sylvania, Danvers, MA) was used for fluorescence excitation and the emitted light was gathered with a dichroic mirror/filter cube (Nikon HYQ Texas Red, Fryer). Images from the fluorescence microscope were collected at a rate of 30 frames/s using a CCD camera (Stanford Photonics, Palo Alto, CA) and recorded on a Sony digital video cassette with a recorder (Sony, B&H Photo-Video, New York, NY). This assembly permits monolayer morphology to be observed over a large lateral area while isotherm data are obtained. The entire assembly is mounted on a vibration isolation table (Newport, Irvine, CA) and controlled by a custom software interface written using LabView 6.1 (National Instruments, Dallas, TX).

Lateral compression experiments. Monolayer spreading solutions of DPPC and POPG (a 7:3 molar ratio) with 10% by weight truncation peptide SP-B (stored in methanol solution to increase solubility) were prepared by dissolving in chloroform (HPLC grade, Fisher Scientific, Pittsburgh, PA) at a concentration of 0.1 mg/ml and adding 0.05 mol% of TR-DHPE. Lipid solutions were stored at $-$20°C in glass vials.

All experiments were performed at 25°C on pure water or 40 wt% glycerol. The monolayer was spread at the gas/water interface by gently depositing drops onto the surface and the organic solvent was allowed to evaporate for 20 min in the case of water or 1 h on the glycerol subphase to allow for equilibration. The barriers were then compressed with a linear speed of 0.1 mm/s, and isotherm measurements in the form of surface pressure (mN/m) vs. area per lipid molecule (Å^2/molecule) were taken at 1-s intervals. The isotherm provides information about the phase behavior of the monolayer as a function of lipid packing density. The surface was imaged continuously with fluorescence microscopy (FM) throughout the compression.

Atomic force microscopy. Higher resolution imaging, i.e., submicron, of the various monolayers transferred from the gas/water interface was obtained with atomic force microscopy (AFM). Following isothermal compression to 55 mN/m, lipid monolayers from the Langmuir trough were transferred onto mica substrates by an inverse Langmuir-Shaefer transfer technique (39). A freshly cleaved mica substrate was placed in a stainless steel apparatus with a surrounding 2 mm high machined knife edge, and the entire setup was placed on the bottom of the trough where it remained submerged in the subphase throughout the compression isotherm. At the desired surface pressure, the subphase was slowly aspirated from the trough to lower the subphase level and the knife edge cut the monolayer as the surface height lowered, preserving monolayer morphology. Drilled holes in the bottom of the steel piece allowed water to exit the chamber completely until the monolayer was deposited on the mica surface. Monolayer morphology before, during, and after transfer was monitored with FM to ensure that the transfer process did not perturb the morphology of the lipid film.

Lipid monolayers transferred to mica substrates were imaged at room temperature using a Multimode Nanoscope IIIA scanning probe microscope (Digital Instruments, Santa Barbara, CA) with a Type J scanner in contact mode in air. Silicon nitride tips NP-S (Veeco Probes, Woodbury, NY), with a nominal spring constant of 0.32 N/m were used; the surface of the tips were decontaminated by UV-generated ozone before sampling (PSD-UV Surface Decontamination System, Novascan, Ames, IA). Substrates were also imaged in tapping mode in air using silicon tips (nominal spring constant of 42 N/m) and minimal force to check for preservation of morphology after imaging in contact mode. As no disruption was found, all substrates were subsequently imaged in contact mode. Images shown were subjected to a first-order plane-fitting procedure to compensate for sample tilt

and, if necessary, to a zeroth-order flattening (raised features were excluded from the flattening calculation).

Surfactant preparations for animal studies. The lipid mixture, used to formulate the synthetic peptides, was based on the known composition of calf lung surfactant lipids (13) and contained (in mg/ml) 16 DPPC, 10 DOPC, 3 POPG, 1 POPE, 3 POPS, and 2 cholesterol, or a total of 35 mg lipids/ml in 150 mM phosphate buffer saline solution (pH 7.0) (59). The lipid mixture alone was used as a negative control. Various synthetic SP-B peptides (1.5 mol%) were formulated in the lipid mixture.

Lavaged rats. The in vivo function of monomeric and dimeric SP-B 1–25 and SP-B 11–25 surfactants were compared with porcine SP-B surfactant and lipids alone in surfactant-deficient rats. The animal experiments were performed with the approval of the Los Angeles Biomedical Research Institute at Harbor-UCLA Medical Center Institutional Animal Care and Use Committee. Anesthesia, surgery, lavage, ventilation, and monitoring used in this study are the same as previously described (8, 23). Briefly, adult male Sprague-Dawley rats weighing 200–225 g were anesthetized with 35 mg/kg sodium pentobarbital and 80 mg/kg ketamine by intraperitoneal injection, intubated, and ventilated with a rodent ventilator (Harvard Apparatus, South Natick, MA) with 100% oxygen, a tidal volume of 7.5 ml/kg, a positive end-expiratory pressure (PEEP) of 3 cmH_2O, and a rate of 60/min. An arterial line was placed in the abdominal aorta for measurements of arterial blood pressure and blood gases. The rats were paralyzed with 1 mg/kg pancuronium bromide intravenously. Only animals with Pa_{O_2} (pressure of O_2 in the airway) values >500 mmHg while ventilated with 100% oxygen were included in the experiments. Their lungs were lavaged eight times with 8 ml of prewarmed 0.9% NaCl and repeated, if necessary, after 15 and/or 30 min until the Pa_{O_2} in 100% oxygen had reached stable values of <100 mmHg, at which point of time the rats were treated with 100 mg/kg of one of the surfactant preparations or lipids only. Lung lavage liquid recovery was ≥95% in all groups. Airway pressures were measured continuously (RSS100-HR pneumotachograph, Hans Rudolph, Kansas City, MI), and arterial blood gases were determined at 15 min intervals throughout the experiments. Blood taken for gas analysis was replaced. After 90 min of ventilation, the rats were killed with 200 mg/kg sodium pentobarbital intravenously. Each treatment group consisted of seven or eight rats.

Data analysis. Oxygenation is reported using the arterial P_{O_2} (mmHg). Dynamic lung compliance was calculated by dividing tidal volume/kg body wt by changes in airway pressure (peak inspiratory pressure minus positive end-expiratory pressure; $ml \cdot kg^{-1} \cdot cmH_2O^{-1}$). Oxygenation and dynamic compliance data are expressed as means ± SE. Between-group comparisons were done by one-way ANOVA followed by the Student-Newman-Keuls multiple comparison procedure. The *t*-test was used for comparisons vs. control values. A *P* value below 0.05 was considered to indicate a significant difference.

RESULTS AND ANALYSIS

Isotherms and fluorescence microscopy. Figure 1 shows the surface pressure vs. molecular area isotherms of the planar monolayers of lung surfactant mixtures, 7:3 DPPC:POPG with various SP-B truncation peptides at 10 wt%, on a pure water subphase at 25°C. This varies from in vivo conditions where the actual composition of the surfactant lining fluid is more viscous, containing the sugary polymer hyaluronic acid and unadsorbed lung surfactant packaged as hyaline (62, 74). It is common in the biophysical lung surfactant literature to use pure water subphases when focusing on the monolayer (15, 21 40, 41, 50); we do explore the role of viscosity briefly at the end of this section. Surface pressure measurements provide information about phase behavior averaged over the entire monolayer surface, and are complemented by direct observation of the monolayer phase morphology with FM, where a small mole percentage of head-labeled lipid dye, TR-DHPE, is added to each monolayer. The bulky headgroup of the dye prefers the liquid expanded (LE) region due to steric effects (35); therefore, condensed (C) domains are dark and the LE or disordered phase is bright. The 7:3 DPPC:POPG lipid monolayer, which has been studied extensively (21), goes through the expected gas (G)/LE coexistence at low lipid density to the pure LE phase at ~90 $Å^2$/molecule, at which point the surface pressure starts to lift off. This is followed by a first-order phase transition, signified by a plateau in the isotherm, where C domains start to form at ~ 18 mN/m, followed by a rapid rise in surface pressure until the collapse of the monolayer at ~70 mN/m. All of the phase changes indicated in the isotherm correlate with phase morphology seen with FM (data not shown). Though POPG is below its critical point and therefore, fluid at 25°C and has a collapse pressure of 48 mN/m, the 7:3 DPPC:POPG binary mixture retains its LE/C biphasic domain structure until collapse where the condensed, dark phase is DPPC rich and the disordered, bright phase at high surface pressures is POPG rich (21). There is a kink in all of the isotherms (including those with SP-B truncation peptides) at ~58 mN/m, which may be attributed to changes in the concavity of the meniscus at the trough barriers; this is not due to POPG squeeze-out because it occurs at a much higher pressure than its collapse pressure.

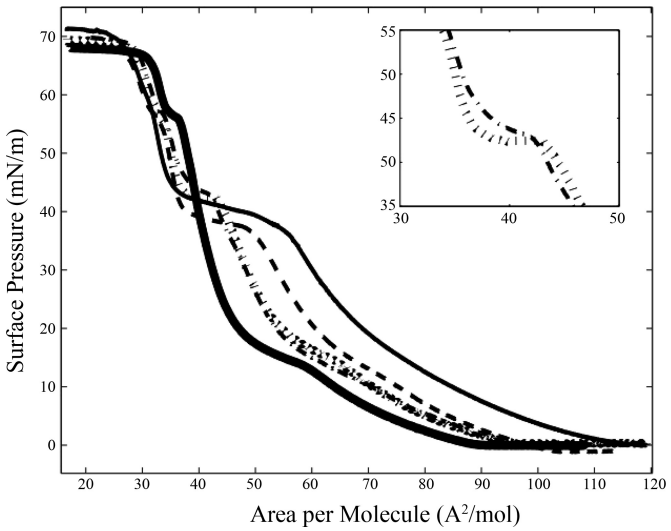

Fig. 1. Surface pressure vs. molecular area isotherms for lung surfactant model mixtures of 7:3 dipalmitoylphosphatidylcholine:palmitoyloleoylphosphatidylglycerol (DPPC:POPG) and various lung surfactant protein B (SP-B) truncation peptides 10 wt%. Thick black line, no peptide; dashed black line, SP-B 1–25; hatched line, SP-B 9–25; dashed dotted line, SP-B 11–25; thin black line, SP-B 1–25Nflex. *Inset*: plateau region of monolayers with SP-B 9–25 and SP-B 11–25. All isotherms were taken on pure water at 25°C.

The four SP-B truncation peptides were chosen to test the functional importance of the NH_2-terminal insertion sequence with SP-B 1–25 serving as a positive control; SP-B 9–25 testing the deletion of the insertion sequence; SP-B 11–25, two residues shorter and lacking the interface-seeking residue 9 tryptophan; and SP-B 1–25Nflex replacing prolines at residues 2 and 4 with alanines to increase the flexibility of the insertion region. Inclusion of each of the SP-B peptides induces obvious changes to the isotherms seen by a higher area per molecule at

lift-off and a second distinct plateau between 35 and 50 mN/m following the first-order phase transition at 18 mN/m. For all the mixtures, collapse (minimum surface tension) occurs at ~70 mN/m. When comparing the effect of the peptides, the plateau appears at the lowest surface pressure for SP-B 1–25 and was longer than that of the smaller truncation peptides, SP-B 9–25 and SP-B 11–25. The plateaus induced by SP-B 9–25 and SP-B 11–25 occur at similar pressures, ~43 mN/m, but inclusion of the two additional residues including tryptophan 9 leads to a longer, flatter plateau region (see Fig. 1, *inset*). The SP-B 1–25Nflex monolayer has a plateau at a pressure intermediate between the peptides with and without the insertion sequence, but of the four species, it has the longest plateau region extending over 25 $Å^2$/molecule. Starting in the plateau region and up to higher pressures, FM images show bright specks of material protruding from the disordered phase of the monolayer down into the subphase (Fig. 2*A*). The plateau, or lack of rise in surface pressure in the isotherm, exists because material is being removed from the film in the form of these bright specks, or three-dimensional nanosilos, while compression is occurring. Since material is going from the two-dimensional interface into the subphase, further compression does not result in a measured pressure increase until material is no longer removed. On decompression of the layer, the small regions of bright fluorescence gradually disappear (Fig. 2*B*), supporting the idea of reversible respreading of the collapsed material. Due to their small length scale, variations in the protrusions or nanosilos caused by different peptides are difficult to distinguish using FM.

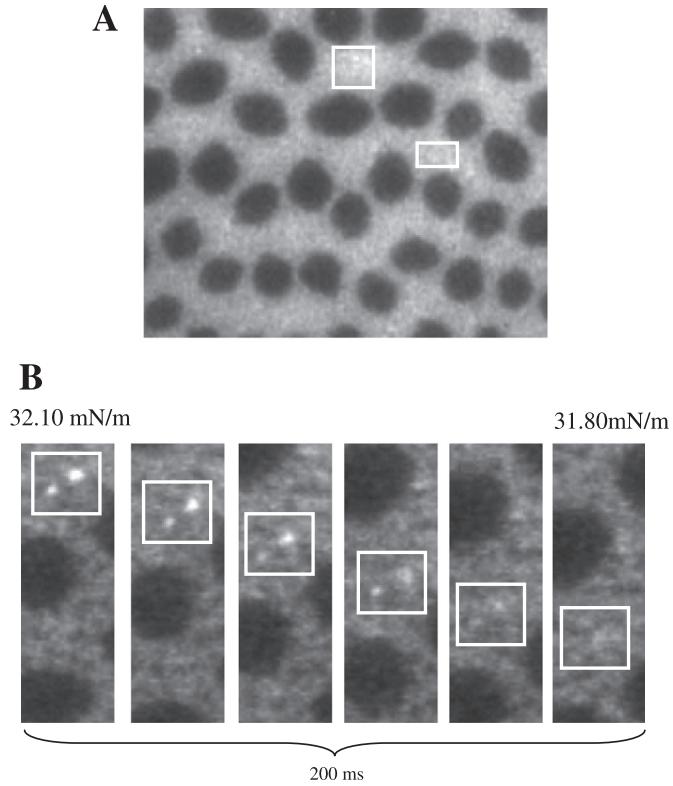

Fig. 2. Fluorescence microscope images of 7:3 DPPC:POPG with 10 wt% SP-B 1–25 (*A*) at a surface pressure of 55 mN/m. Note the speckles of increased intensity (nanosilos) in the bright phase. *B*: on decompression, fluorescent speckles gradually disappear, indicating reversible respreading of the collapsed material stored in the nanosilos into the lipid monolayer.

Atomic force microscopy. To understand how the different truncation peptides affect the formation of nanosilos or reversible repositories for fluid lipids at high surface pressures and correlate this with characteristics of the plateaus in the corresponding isotherms, monolayers were deposited at 55 mN/m on mica substrates through a modified Langmuir-Schaefer method (39). The monolayers were imaged with FM before, during, and after deposition to ensure that membrane morphology was preserved. The surface pressure of 55 mN/m was chosen because it is past the point of nanosilo formation and the structures should be stable. After the monolayers were deposited onto mica substrates, they were imaged with AFM using contact mode in air to obtain a detailed nanometer-scale picture of how SP-B peptide length affects the formation of these structures.

A deposited monolayer of 7:3 DPPC:POPG (Fig. 3*A*) shows C domains in the lower left and right corners interspersed with the more disordered LE phase between them. Section analysis supports this assignment with a height difference of ~0.8 nm between the two phases, consistent with that reported in the literature for the difference between condensed and fluid lipid phase domains as measured with AFM (26). While the corresponding FM images (data not shown) of the pure lipid monolayer at the same pressure show large, round condensed domains embedded in a bright liquid expanded matrix, the deposited monolayer shows a considerable amount of condensed lipid in the bright, fluid region. The effect of these nanoscale condensed domains on the membrane's material properties has been discussed in a previous paper (50).

In the 7:3 DPPC:POPG model lung surfactant mixture with 10 wt% SP-B 1–25, there are numerous protrusions of material from the fluid region, ranging from 200 to 400 nm in diameter, and 5 to 20 nm higher than the surrounding monolayer (Fig. 3*B*). Nanosilo heights were carefully characterized at four different locations within an individual deposited monolayer sample and this analysis was performed on a minimum of three separate samples. The exact number of nanosilos used in each height estimation varied with their surface density (Fig. 3B-E). The repositories occur at height steps of 5 ± 1 nm such that nanosilo heights above the monolayer background are 5 ± 1, 10 ± 1, 15 ± 1, 20 ± 1 nm. This echoes previous experiments of a 3:1 DPPG:POPG monolayer containing SP-B 1–25 where the nanosilos occur at heights corresponding roughly to multiples of the bilayer thickness of POPG (14, 63). The protrusions are round and smooth and exhibit edges reminiscent of a cylinder of material extruded into the subphase. Deletion of the NH_2-terminal insertion sequence leads to a markedly different monolayer morphology. For the 7:3 DPPC:POPG SP-B 9–25 monolayer, the protrusions are higher in density and profuse in any region of the film containing fluid phase (Fig. 3C). The dimensions of the nanosilos in the SP-B 9–25 film were 50–200 nm in width, but only 5 nm tall, approximately the height of a single bilayer. Removal of the next two residues including the proposed membrane-seeking tryptophan, with SP-B 11–25, leads to low density protrusions 50–350 nm in width, but only ~2 nm in height, or roughly the thickness of a single monolayer (Fig. 3*D*). In both the 9–25 and 11–25 cases, the edges of the nanosilos were not smooth and round, indicating more fluctuations or lower stability of the structure in the subphase compared with those created by SP-B 1–25. Inclusion of the SP-B 1–25Nflex peptide (Fig. 3*E*) results in a

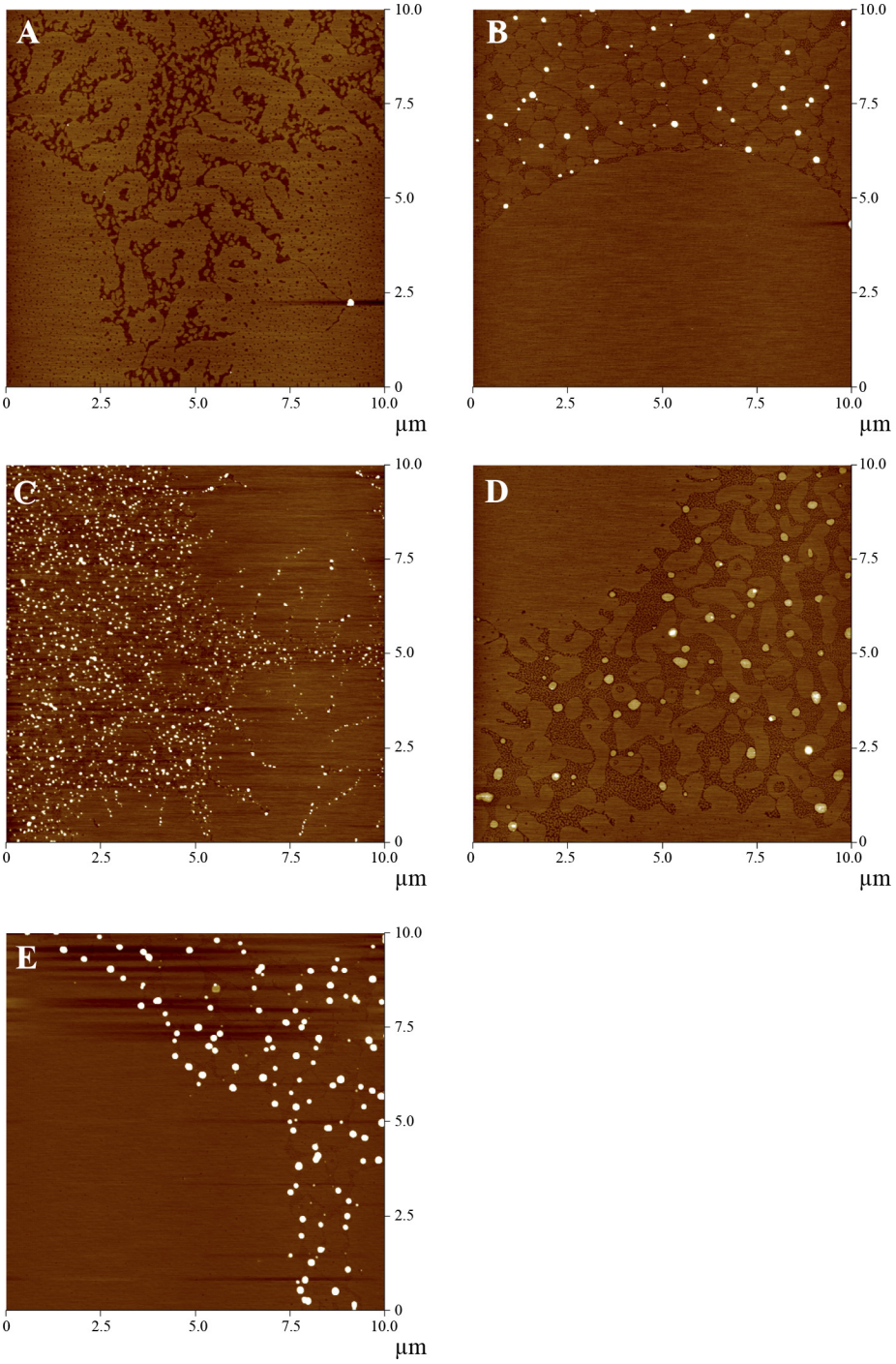

Fig. 3. Atomic force microscopy (AFM) topographic images of 7:3 DPPC:POPG monolayers containing 10 wt% SP-B truncation peptides transferred at 55 mN/m from a water subphase at 25°C (z-scale 5 nm). *A*, no peptide; *B*, SP-B 1–25; *C*, SP-B 9–25; *D*, SP-B 11–25; *E*, SP-B 1–25Nflex.

monolayer morphology similar to that with SP-B 1–25 peptide except the nanosilos on average are of higher density and have a maximum height of ~30 nm.

Effect of peptide concentration. All of the previously discussed experiments used 7:3 DPPC:POPG lipid monolayers with 10 wt% peptide because this is a typical concentration to obtain comparable surface activity of the SP-B 1–25 with that of the native protein. In the case of the shortest peptide, SP-B 11–25 (mw = 1,697 g/mol), this would result in twice the concentration of membrane interacting amphipathic helices compared with SP-B 1–25 (mw = 3,340 g/mol). Therefore, parallel experiments were run with peptides (9–25 and 11–25) using a mol%, which correlated to the same mole fraction as 10 wt% SP-B 1–25, and no qualitative differences were seen in the isotherm plateau region or the height of the resulting nanosilo structures. Since Ding et al. (15) reported a correlation between nanosilo size and SP-B 1–25 concentration, these results indicate a saturation concentration of the shorter truncation peptides (9–25 and 11–25) at ~0.5 mol% such that any further addition of peptide does not affect or improve its ability to support these repositories. The insertion sequence is therefore a necessary and important region of the peptide in terms of

nanosilo formation and maintenance of material close to the interface at low surface tensions.

Glycerol subphase. In most cases, model lung surfactant monolayer experiments are run on aqueous subphases with the inclusion of electrolytes to better model physiological conditions. However, to properly model the lung lining, one needs to take into account that the alveolar lining fluid between the alveolar sac and the lung surfactant is approximately one-tenth of a micrometer in thickness. Therefore, its hydrodynamics are dominated by thin film physics where effective viscosity is larger than that in bulk fluid (74). To raise the viscosity beneath the monolayer, parallel experiments were run on a 40 wt% glycerol subphase. To best illustrate the effect of a glycerol subphase, monolayers that formed tall, dense nanosilos on water, the SP-B 1–25 and the 1–25Nflex peptides, were deposited. In both cases (Figs. 4, *A1* and *B*), the protrusions of material were reduced in width and also in height, to ~5 nm above the surrounding monolayer. It should be noted that while these AFM images are intrinsically noisier due to the adherent glycerol subphase (see 5 μm scan in Fig. 4*A2*), the measured heights were reproducible across samples.

Rat studies. The efficacy of the truncation peptides was tested in vivo. Porcine SP-B in combination with lung surfactant lipids was used as the benchmark for comparison while lipids alone were the negative control. The NH_2-terminal SP-B sequence, SP-B 1–25, and the shortest truncation peptide, SP-B 11–25, in monomer and dimer forms were used to test the importance of the NH_2-terminal insertion sequence. Rats demonstrated a rapid recovery of oxygenation (Pa_{O_2}) and dynamic compliance (tidal volume/kg body wt) after rescue treatment with porcine SP-B and monomeric and dimeric SP-B 1–25 surfactant, but not with monomeric and dimeric SP-B 11–25 surfactant or lipids alone (Figs. 5 and 6). The average arterial P_{O_2} values following lung lavage were 13% of the prelavage values and increased after treatment with porcine SP-B, monomeric and dimeric SP-B1–25, monomeric and dimeric SP-B 11–25 surfactant, and lipids alone to 80%, 56%, 64%, 18%, 19%, and 20% of the prelavage values, respectively. Postlavage dynamic compliance dropped to 61% of the prelavage values and increased after treatment with porcine SP-B, monomeric and dimeric SP-B1–25, monomeric and dimeric SP-B 11–25 surfactant, and lipids alone to 82%, 73%, 77%, 65%, 65%, and 69% of the prelavage values, respectively. Arterial P_{O_2} values for porcine SP-B surfactant were significantly higher than those of monomeric and dimeric SP-B1–25 surfactant, which were higher than those of monomeric and dimeric SP-B11–25 surfactant and lipids alone when tested with one-way ANOVA ($P < 0.001$). Dynamic compliance values for porcine SP-B and monomeric and dimeric SP-B1–25 surfactant exceeded those of monomeric and dimeric SP-B11–25 surfactant and lipids alone ($P < 0.005$). These results show that the NH_2-terminus is important for SP-B function.

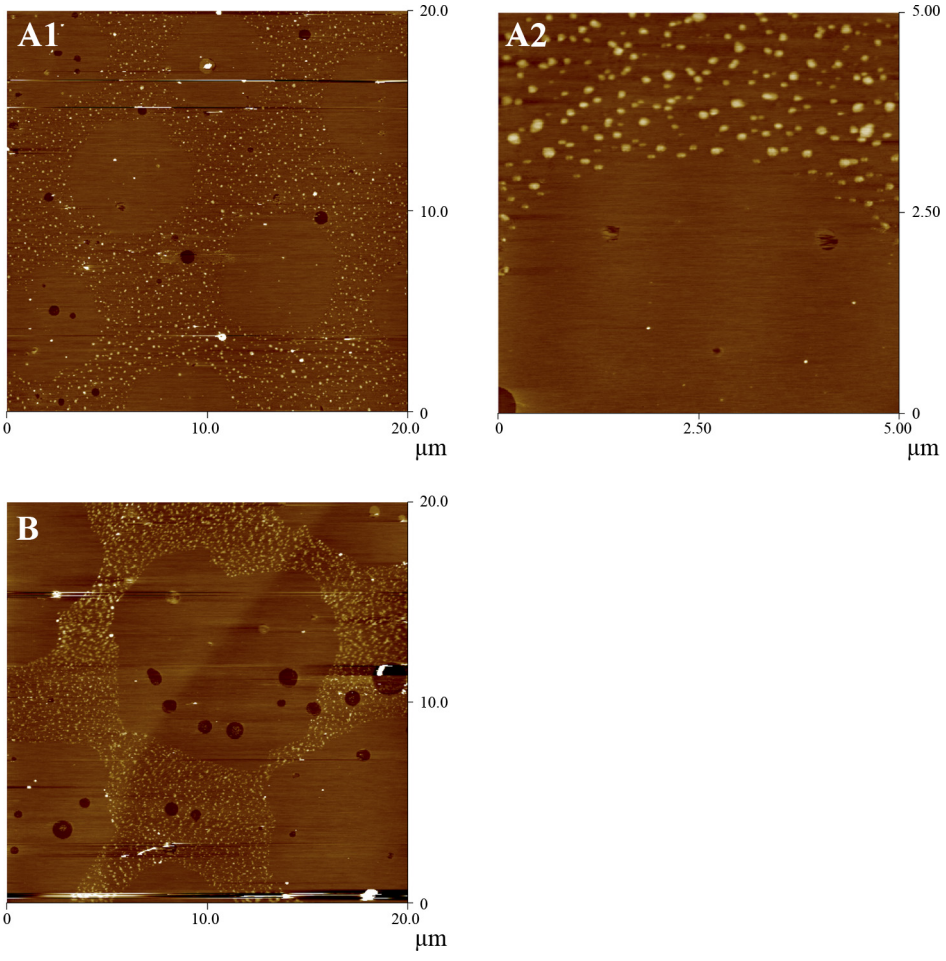

Fig. 4. AFM topographic images of 7:3 DPPC:POPG monolayers with 10 wt% (*A1* and *A2*) SP-B 1–25 and (*B*) SP-B 1–25Nflex monolayers transferred at 55 mN/m from a 40 wt% glycerol subphase at 25°C (z-scale 5 nm). All nanosilos are ~5 nm above the height of the monolayer.

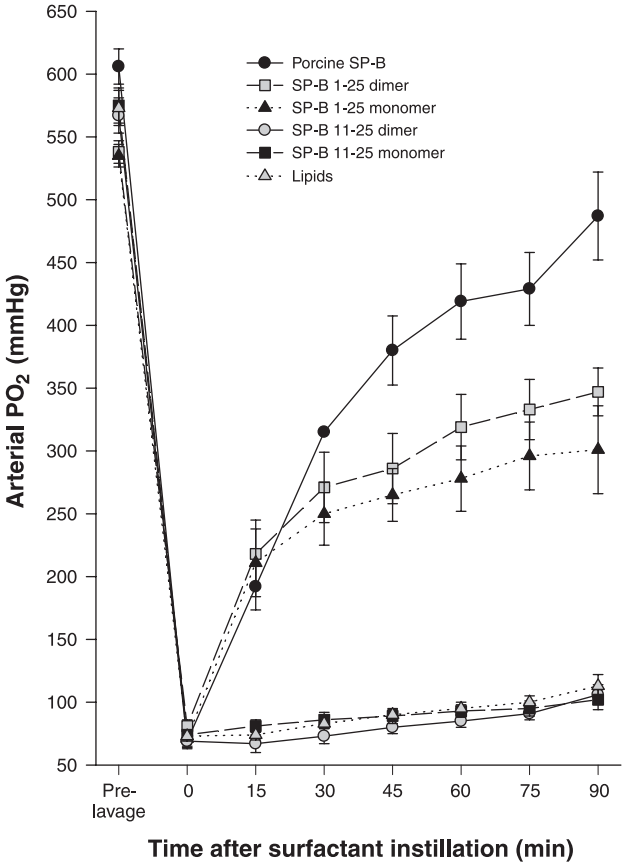

Fig. 5. Oxygenation, expressed as arterial Po_2 (mmHg), in rats treated with porcine SP-B surfactant (positive control), lipids (negative control), and the four experimental surfactant preparations with monomeric or dimeric SP-B 1–25 and SP-B 11–25 peptides. The differences between porcine SP-B surfactant and monomeric and dimeric SP-B 1–25 surfactant and the differences between SP-B 1–25 and SP-B 11–25 surfactants or lipids alone are significant ($P < 0.001$).

DISCUSSION AND CONCLUSIONS

Proper pulmonary function requires low surface tension at the end of expiration to minimize the work of breathing, but the lung surfactant monolayers lining the alveoli must also be fluid enough to respread rapidly during the expansion of the interface that accompanies inspiration. As reported in several previous papers (14, 15, 37), inclusion of the SP-B protein in lung surfactant mixtures helps with the formation of a reservoir of surfactant attached to the interface, which keeps material in close proximity to the film at low surface tensions, facilitating the squeeze-out of more fluid components on compression and the reinsertion of the surface active material on expansion.

In the isotherms of the model lung surfactant mixtures (Fig. 1), the lift-off from G to LE phase occurs at a higher area per molecule with the addition of SP-B peptides compared with the pure lipid system. This agrees with previously published results (14, 15, 57) and occurs because the surface-active peptide occupies space at the gas/water interface. All monolayers deposited below 35 mN/m showed no evidence of nanosilos as measured by AFM (data not shown). This indicates that the plateau at 45 mN/m can be attributed to interactions between fluid POPG and SP-B truncation peptides, leading to the formation of nanosilos (visualized by FM in Fig. 2). In previous studies of model lung surfactant mixtures using saturated lipid systems such as DPPC:DPPG, nanosilo heights were 5 nm (14, 15), but inclusion of unsaturated lipid, such as POPG, increased the protrusion height to tens of nanometers (14, 63). Nanosilo height and density is therefore dependent on the lipid system, with more rigid monolayers having lower resulting heights. Extrusion of a cylinder of material is easier from a more disordered, fluid region compared with a more tightly packed monolayer.

Comparison of isotherm and AFM measurements. The peptide that most closely resembles that of native SP-B, SP-B 1–25, has a relatively long plateau at ~45 mN/m in its isotherm and this correlates with stable, tall (up to 20 nm) nanosilos as imaged with AFM. The length of the induced plateau provides information about the height and quality (degree of regularity of the cylindrical structure) of the nanosilo formation because a longer plateau at a relatively stable surface pressure indicates a larger fraction of material is removed from the monolayer. The length of the SP-B 1–25 plateau shows that 3 nanoliters of material were lost provided that the lipid volume was preserved. From the AFM data, the volume of the nanosilos in the SP-B 1–25 monolayer, estimated based on surface coverage and height of the cylindrical nanosilos, is in the range of 0.3–5.29 nanoliters. This estimate

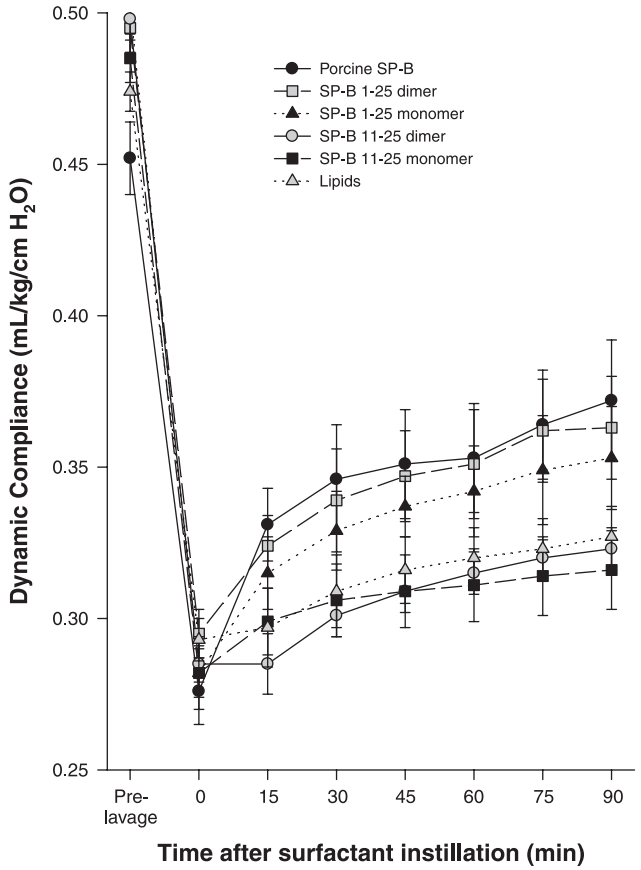

Fig. 6. Dynamic compliance (ml · kg^{-1} · cmH_2O^{-1}) in rats treated with porcine SP-B surfactant (positive control), lipids (negative control), and the four experimental surfactant preparations with monomeric or dimeric SP-B 1–25 and SP-B 11–25 peptides. The differences between porcine SP-B surfactant, monomeric and dimeric SP-B 1–25 surfactant, and monomeric and dimeric SP-B 11–25 surfactants or lipids alone are significant ($P < 0.005$).

is calculated based on the statistical distribution of the nanosilos and the range of nanosilo size. The agreement between the techniques shows that most of the lipid being removed at the 45 mN/m isotherm plateau is being extruded into nanosilos.

While both peptides missing the insertion sequence have similar plateaus in their respective isotherms, the nanosilos in the SP-B 9–25 monolayer have higher surface coverage across the interface and were approximately the height of a lipid bilayer above the surrounding deposited monolayer as opposed to the SP-B 11–25 monolayer-thick nanosilos. The insertion sequence is instrumental in the formation of nanosilos, but the 2 amino acid difference between the 9–25 and the 11–25 peptides has also proven to be dramatic. While the difference in peptide lengths may have geometric or other structural effects that could potentially affect the activities of the two peptides, the loss of the membrane anchoring tryptophan in the 11–25 peptide is likely to also contribute to the functional differences observed. In both cases, the nanosilos are not as round or cylindrical as those in the 1–25 monolayer and this may be attributed to less symmetric formation of nanosilos or an unstable attachment of the structure to the monolayer causing greater disruption on deposition to the solid substrate. In either case, nanosilo height and quality are compromised by the deletion of the insertion sequence.

The inclusion of SP-B 1–25Nflex (P2,4A) peptide results in the longest plateau in the isotherm, the tallest of the nanosilo structures, and high nanosilo density. Replacement of the proline residues with alanine ones increases the flexibility of the insertion sequence because proline amino acids tend to reduce conformational freedom since the side chain is fixed via an extra covalent bond to the main chain. This suggests that a more flexible insertion sequence is better able to stabilize the formation of nanosilos. These data are in contrast to studies where amino acid substitutions of alanine for prolines 2, 4, and 6 (P2,4,6A) in a slightly longer NH_2-terminal SP-B peptide model (SP-B 1–37) decrease the appearance of a plateau at 45 mN/m in the isotherm, potentially due to lack of nanosilo formation (57). This was further supported by an expansion isotherm with P2,4,6A showing less reinsertion of surface active material into an expanding film. The differences seen compared with our isotherm results may be due to the length difference of the peptide (SP-B 1–37 vs. SP-B 1–25) and the fact that proline 6 may significantly contribute to native SP-B activity.

Proposed model. This work echoes results from previous studies with quantized nanosilo height and a propensity for the nanosilo repository to grow from monolayer regions enriched in anionic fluid lipids (14, 15, 37, 63). Furthermore, these data indicate that the propensity for nanosilo formation is correlated to SP-B peptide structure. In this section, we provide a model of nanosilo growth.

A key biophysical component to proper lung surfactant function is reversible collapse. Collapse has been well studied in rigid lipid monolayers that can be modeled as thin elastic sheets (4). Lipids in such monolayers are well packed and move only through large micrometer sized correlated displacements that can be predicted using general scaling laws (4). The behavior of fluid monolayers at collapse is far less understood, with experiments (21) and recent MD simulations (49) showing that collapsed fluid lipids tend to aggregate into smaller scale local structures, or disks that transform into vesicles. Fluid collapse structures are clearly Brownian particles (sensitive to local thermal fluctuations) that diffuse from the interface in a short time span (21). Surfactant protein can help "anchor" anionic fluid lipids like POPG to the interface once they are removed from the surface at high compressions (14, 15, 37, 63). Our work provides a functional understanding of the SP-B NH_2-terminal insertion sequence beyond anchoring the protein to the two-dimensional membrane lining the lung, as it also stabilizes the formation of nanosilos, a unique non-Brownian surface associated reservoir for fluid lipids different from vesicular structures seen in lipid only systems.

Recent simulations show the evolution of vesicles from lipid disks beneath a monolayer is driven by minimization of line energy that exists around the perimeter of the disk (49). Models of vesicle formation show that a suspension of lipids initially organizes into spherical micelles that grow into flat bicelles or discoid micelles. As the bicelles grow, they curve to eventually form a closed spherical shell or a vesicle (18, 19). These transitions are driven by the strong entropic tendency for lipid hydrophobic tails to aggregate and separate themselves from water. Lipid headgroup geometry also imposes restrictions onto the structures that grow. For quasi-cylindrical lipids such as POPG and DPPC, where the cross-sectional areas of headgroup and tail are similar, flat bilayered structures prevail (65). The overall energy of a bilayer disk contains another term: the edge energy (19, 52). Hydrocarbon tails belonging to lipids toward the center of a disk are well shielded from the surrounding water, but the shielding breaks down at the outer edge of the disk (Fig. 7*A*; 65, 68). This breakdown comes from the frustration that develops when lipid molecules try to curve around the disk edge (Fig. 7*B*; 19, 65). Molecules like DPPC and POPG that optimize their packing geometry best in flat bilayers do a poor job packing around sharp curves, leaving exposed hydrocarbon tails at the bicelle edge (52, 65, 68). The

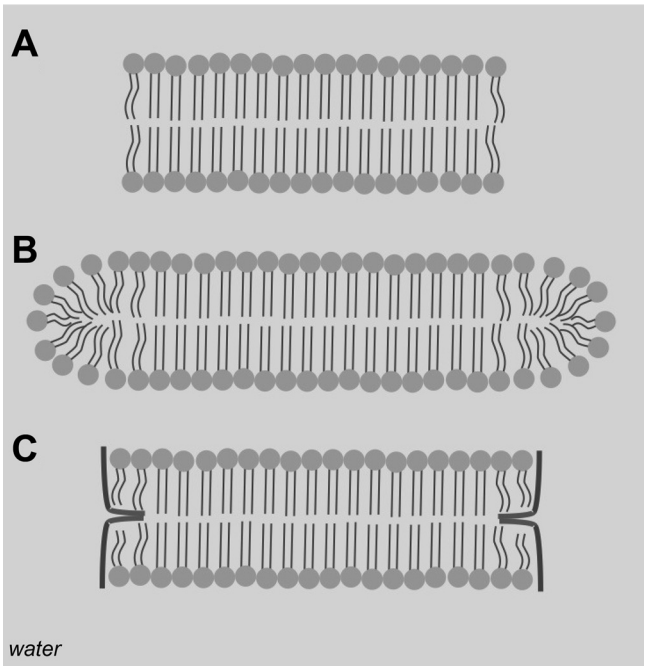

Fig. 7. Cross-sectional view of bicelle structures. *A*, unstable structure where the edge is exposed to water; *B*, edge stabilized by more fluid, shorter tailed lipids; *C*, edge stabilized by amphiphilic peptide.

edge energy is given as the product of the line tension (energy density at water/bicelle edge interface) and the bicelle circumference: $\gamma \times L$ (18, 19). Since the bicelle circumference grows linearly with diameter, the edge energy increases with disk size. To minimize the edge energy, bicelles may bend into spherical caps; this decreases the rate of edge growth at the expense of disturbing optimal packing at the bicelle center (18). The energy of bending the bicelle is the product of bending stiffness [measurements put this value in the range of $\kappa \sim 25$–50 kT (7)] and the curvature of the deformed surface (18). Balancing the edge energy and the energy of bending provides an upper size limit for a discoid bicelle: $R_{max} \sim 4\kappa / (\gamma \times t)$, where t is the thickness of the bicelle, κ is the bending energy, and γ is the line tension (18, 19). When $R < R_{max}$, a flat discoid bicelle is stable, but for $R > R_{max}$, the bicelle begins to deform into a vesicle. The R_{max} relation shows that the two primary ways of increasing the bicelle size are by stiffening the bicelle or decreasing its line tension.

In model lung surfactant systems, experiments (21) and simulations (49) clearly show that lipid only bicelles transform into vesicles, which end up detaching from the monolayer. Nanosilos however, are formed from large (>50 nm) discoid bicelles that remain associated with the monolayer, do not transform into vesicles, and with the inclusion of the correct peptide, stack one upon each other. The peptide clearly plays an important role in stabilizing the discoid bicelle mesophase and thus prevents the transition into vesicles that lead to irreversible lipid loss by diffusion.

Building on the understanding of the bicelle-vesicle transition, we propose that the lung surfactant peptide stabilizes POPG enriched bicelles by attaching at the bicelle edge and thus lowering the line tension (Fig. 7*C*). Polarization modulation infrared reflectance absorption spectroscopy of the SP-B 1–25 peptide in 4:1 DPPC:DOPG monolayers shows a reorientation of the peptide from parallel to perpendicular with respect to the interface at high compression (59), placing the peptide in a configuration that would support extrusion of discoid bicelles. Moreover, the amphipathic helix region of SP-B, estimated to span at least 8 amino acids (residues 14–21) (38), is ~12 Å in length while the lipid tail region in the bilayer spans ~20 Å (73), suggesting that two helices could comfortably span the length of the tail region of the bilayer as outlined in Fig. 7*C*. The propensity for a particular surfactant peptide to adsorb to the bicelle edge determines the degree to which it can lower the line tension (19). Given our data that nanosilos formed from monolayers containing SP-B with its hydrophobic insertion sequence can be nearly ten times as large, we conclude that the insertion sequence significantly augments the adsorption of lung surfactant peptide to the nanosilo edge increasing the stability of the structure. Figure 8*A* provides a model of how the insertion sequence may interact with the bicelle edge, providing an anchor for the peptides around the bicelle perimeter. Not having this anchor (Fig. 8*B*) prevents the peptides from lowering the line tension as effectively, thus leading to shorter bicelles as seen with SP-B 9–25 and 11–25. Following this argument, the more flexible insertion sequence of the 1–25Nflex likely inserts more easily or anchors more securely in the hydrophobic portion of the membrane leading to more stable, hence larger bicelles.

Veldhuizen et al. (67) suggested that the dimerized version of the peptide (dSP-B 1–25 where the two monomers are joined by a disulfide linkage at cysteine 8) functions efficiently in surface analysis assays because one-half of the dimer can be associated with the monolayer at the air/water interface whereas the other one-half stabilizes the nanosilo, but with heights of nanosilos stemming up to 30 nm as seen in our AFM measurements, this is unlikely to be the case. Both in vivo (shown here) and in vitro studies of dSP-B 1–25 show that a dimerized version of the peptide better approximates the functionality of the full-length SP-B protein compared with the SP-B monomer (14, 69, 70). On the basis of the present results, we propose that the dimer has amphipathic helices held stably together via a disulfide bond with a long enough span to hold the lipid bilayers within the bicelle stacks tightly together while the insertion sequence anchors the peptide to the nanosilo; this assists in reversibility during expansion when the monolayer surface tension rises. This proposed splayed structure of the helix dimer is supported by Raman and polarized FTIR spectroscopy studies performed on the SP-B 1–25 and SP-B 8–25 disulfide linked dimer. While the disulfide linkage is strained, it can clearly permit dimer helical splays and surface dependent helix orientation in surfactant lipids, in agreement with our proposed model (6). Additionally, recent work on lung surfactant peptoids, or peptide mimics, showed that the linkage of monomers by a rigid triazole moiety to form a dimer enhanced in vitro surface activity in a lipid film relative to its monomeric counterparts (16). This further supports the idea that close proximity of the 2 peptoid helices serves to stabilize nanosilo formation. In surfactant-deficient animals, deletion of both the insertion sequence and the tryptophan membrane anchoring

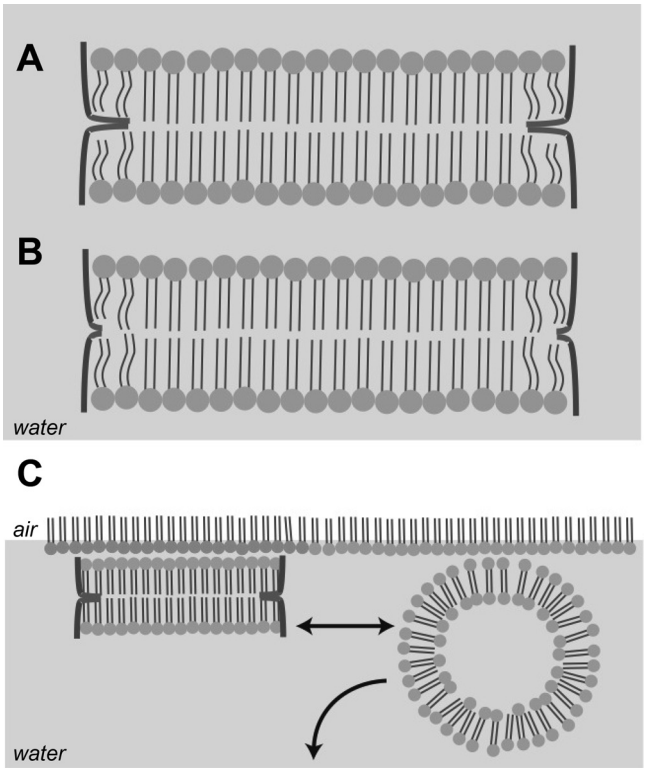

Fig. 8. Proposed bicelle structures for SP-B 1–25 and 1–25Nflex (*A*); SP-B 9–25 (*B*). Note the NH_2-terminal insertion sequence is anchored between the 2 layers of the bilayer. *C*: comparison of stable bicelle nanosilo to fluid lipid vesicle.

residue results in relative oxygenation and lung compliance similar to that of lipids alone. This is true even in the case of the dimerized SP-B 11–25 connected by a disulfide linkage at position 11, which suggests that the extended helix of an SP-B dimer is not sufficient for nanosilo formation, and hence, animal survival depends on the inclusion of a insertion sequence to anchor it into the membrane.

A still unresolved question is why bicelles stack on each other forming nanosilos and why such structures remain attached to the interface. As to the first point, the formation of stacks as superstructures has been observed before in bulk solutions of lipid discoid bicelles (58). Furthermore NMR experiments with bicelle solutions have shown a strong propensity for spontaneous alignment of bicelles in a magnetic field (52, 65, 68). This leads to the possibility that because of its discoid structure, the bicelle has macroscopic electromagnetic dipoles oriented along preferred directions with respect to its long and short axes. Therefore, dipole coupling could drive bicelle stacking. As material is being expelled from the two-dimensional interface on compression, it is generally favored (in the case of SP-B with an NH_2-terminal insertion sequence) to add to the height of a nanosilo rather than nucleate another at a new location. The same line of reasoning could be used to explain why bicelles remain so strongly attached to the surface. Unlike vesicles, bicelles have a large surface area to interact with the monolayer (Fig. 8*C*). As a vesicle grows, the area of contact between the vesicle and surface decreases, leaving an ever-smaller surface tether that must resist constant thermal fluctuations. Eventually thermal forces overcome the strength of the attachment to the monolayer, leading to vesicle detachment and diffusion from the surface as seen in experiments and simulations (21, 49). Conversely, bicelle growth leads to an increasing contact area with the surface, and larger bicelles have a stronger surface attachment capable of resisting thermal forces driving lipid detachment from the interface.

Glycerol subphase. Monolayers with SP-B 1–25 and SP-B 1–25Nflex on water show nanosilos upwards of 20-nm tall, corresponding to the height of multiple stacked bicelles. In our attempt to make Langmuir trough experiments more physiological, the subphase was changed to mimic the ~12 mPa/s viscosity of the alveolar lining fluid (74), which is one order of magnitude higher than the dynamic viscosity of 0.89 mPa/s for water at 25°C. This was accomplished by making aqueous solutions of 40 wt% glycerol with an effective viscosity of 3.18 mPa/s; such a subphase was used because a subphase with any higher weight percentage glycerol (e.g., 64% to match the 12 mPa/s of the lung lining) would make AFM imaging technically challenging due to strong adhesive forces between the sample and tip. On a glycerol subphase, the nanosilo height was reduced to a single bilayer (5 nm) for both peptides. A possible explanation for this reduction in nanosilo height is viscous drag. As the nanosilo forms and grows, it can be modeled as a disk pushing into the subphase. The viscous drag force experienced by a typical SP-B 1–25 nanosilo is $F = 16 \eta R u$, where radius $R = 200$ nm, η is the dynamic viscosity of the subphase, and u is the velocity of nanosilo growth. The velocity is calculated by distance traveled (nanosilo height) and estimating a time over which the nanosilo develops. Nanosilo reincorporation events captured by FM take several camera frames to complete (Fig. 2*B*), such that formation of nanosilos likely occurs on the order of milliseconds (assume an upper boundary value of 1 s for simplicity). The viscosity of water is ~1 mPa/s, 40% glycerol ~3 mPa/s, and pure glycerol ~1,000 mPa/s. The drag force experienced by a nanosilo moving 20 nm into a water subphase is on the order of 1×10^{-17} N. The work required can be estimated by multiplying this force by distance traveled, again 20 nm, giving 0.0003 kT. The drag force in 40% glycerol is 3×10^{-17} N and in pure glycerol 1×10^{-13} N; and the corresponding amount of work required is 0.001 kT and 0.3 kT, respectively. The noteworthy result of this analysis is that even in pure glycerol, the amount of energy required to work against viscous drag is less than thermal energy available to the system (1 kT).

Another way of looking at this is to calculate the mean free path that a typical bicelle would travel in the different subphases away from the interface under the influence of only thermal forces. The mean-free path is given by $r = (6Dt)^{1/2}$, where t is the time allowed for motion, and the diffusion coefficient, D, can be estimated using the Einstein formula D = Tb, T is absolute temperature and b, the mobility [defined as $(16 \eta R)^{-1}$ for our bicelle]. In water, the mean free path of a 200 nm bicelle is >2 μm and in pure glycerol it is around 100 nm. Clearly thermal energy is high enough to move the small nanosilos far from the monolayer in various subphases. This simple analysis indicates that a strong adhesion force (potentially electromagnetic as mentioned earlier) must exist between nanosilos and the surface monolayer. Furthermore, the suppression of nanosilo growth in glycerol solutions cannot be attributed only to viscous drag; the effect of glycerol subphases on the properties of the lipid film will be the subject of future work.

The in vitro monolayer compression and deposition experiments show that the insertion sequence of SP-B, the NH_2-terminal residues 1–8, is necessary for the SP-B 1–25 construct to form nanosilos of greater than one bilayer in thickness, further illustrating the role of SP-B in stabilizing reversible nanosilo structures and at suppressing the formation of vesicles. Our results indicate that the formation of tall, stable nanosilos in vitro correlates to in vivo efficacy in animals with induced RDS providing further insight into the minimal structural constructs necessary for a SP-B mimic.

GRANTS

This work was supported in part by the University of Chicago Materials Research Science and Engineering Center program of the National Science Foundation (DMR 0820054). S. L. Frey is grateful for the support of a National Science Foundation Graduate Research Fellowship. L. Pocivavsek thanks the University of Chicago Medical Scientist Training Program for support. F. J. Walther and A. J. Waring are supported by National Heart, Lung, and Blood Institute Grants HL-55534-10 and HL-92158-02. K. Y. C. Lee is grateful for support from March of Dimes (No.6-FY07-357) and the US-Israel Binational Science Foundation (No. 2006076).

DISCLOSURES

No conflicts of interest are declared by the authors.

Present address of S. L. Frey is Department of Chemistry, Gettysburg College in Gettysburg, PA.

REFERENCES

1. **Anzueto A, Baughman RP, Guntupalli KK, Weg JG, Weidemann HP, Raventos AA, Lemaire F, Long W, Zaccardelli DS, Pattishall EN.** Aerosolized surfactant in adults with sepsis-induced acute respiratory distress syndrome. *N Engl J Med* 334: 1417–1421, 1996.

2. **Avery ME, Mead J.** Surface properties in relation to atelectasis and hyaline membrane disease. *Am J Dis Child* 97: 517–523, 1959.
3. **Baatz JE, Zou Y, Cox JT, Wang Z, Notter RH.** High-yield purification of lung surfactant proteins SP-B and SP-C and the effects on surface activity. *Protein Expr Purif* 23: 180–190, 2001.
4. **Baoukina S, Monticelli L, Risselada HJ, Marrink SJ, Tieleman DP.** The molecular mechanism of lipid monolayer collapse. *Proc Natl Acad Sci USA* 105: 10803–10808, 2008.
5. **Berggren P, Curstedt T, Grossmann G, Nilsson R, Robertson B.** Physiological activity of pulmonary surfactant with low protein content: effect of enrichment with synthetic phospholipids. *Exp Lung Res* 8: 29–51, 1985.
6. **Biswas N, Waring AJ, Walther FJ, Dluhy RA.** Structure and conformation of the disulfide bond in dimeric lung surfactant peptides SP − $B_{1–25}$ and SP − $B_{8–25}$. *Biochim Biophys Acta Biomembranes* 1768:1070–1082, 2007.
7. **Boal B.** *Mechanics of the Cell.* Cambridge, UK: Cambridge University Press, 2002, p. 159.
8. **Brackenbury AM, Malloy JL, McCaig LA, Yao LJ, Veldhuizen RAW, Lewis JF.** Evaluation of alveolar surfactant aggregates in vitro and in vivo. *Eur Respir J* 19: 41–46, 2002.
9. **Bruni R, Taeusch HW, Waring AJ.** Surfactant protein B-lipid interactions of synthetic peptides representing the amino-terminal amphipathic domain. *Proc Natl Acad Sci USA* 88: 7451–7455, 1991.
10. **Clark JC, Wert SE, Bachurski CJ, Stahlman MT, Stripp BR, Weaver TE, Whitsett JA.** Targeted disruption of surfactant protein B gene disrupts surfactant homeostasis, causing respiratory failure in newborn mice. *Proc Natl Acad Sci USA* 92: 7794–7798, 1995.
11. **Creighton TE.** *Proteins: Structures and Molecular Properties* (2nd ed.). New York, NY: Freeman. 1993, p. 176–177.
12. **Cruz A, Casals C, Plasencia I, Marsh D, Pérez-Gil J.** Depth profiles of pulmonary surfactant protein B in phosphatidlycholine bilayers studied by fluorescence and electron spin resonance spectroscopy. *Biochemistry* 37: 9488–9496, 1998.
13. **Curstedt T, Johansson J.** New synthetic surfactant—how and when? *Biol Neonate* 89: 336–339, 2006.
14. **Diemel RV, Snel MME, Waring AJ, Walther FJ, van Golde LMG, Putz G, Haagsman HP, Batenburg JJ.** Multilayer formation upon compression of surfactant monolayers depends on protein concentration as well as lipid composition—an atomic force microscopy study. *J Bio Chem* 277: 21179–21188, 2002.
15. **Ding J, Doudevski I, Warriner HE, Alig T, Zasadzinksi JA, Waring AJ, Sherman MA.** Nanostructure changes in lung surfactant monolayers induced by interactions between palmitoyloleoylphosphatidlyglycerol and surfactant protein B. *Langmuir* 19: 1539–1550, 2003.
16. **Dohm MT, Seurynck-Servoss SL, Seo J, Zuckermann RN, Barron AE.** Close mimicry of lung surfactant protein B by "clicked" dimmers of helical, cationic peptoids. *Biopolymers*, Epub. DOI:doi: 10.1002/bip.21309.
17. **Frey SL, Lee KYC.** Temperature dependence of poloxamer insertion into and squeeze-out from lipid monolayers. *Langmuir* 23: 2631–2637, 2007.
18. **Fromherz P.** Lipid-vesicle structure: size control by edge-active agents. *Chem Phys Lett* 94: 259–266, 1983.
19. **Fromherz P, Rocker C, Ruppel D.** From discoid micelles to spherical vesicles: the concept of edge activity. *Faraday Discuss* 81: 39–48, 1986.
20. **Glasser SW, Burhans MS, Korfhagen TR, Na CL, Sly PD, Ross GF, Ikegami M, Whitsett JA.** Altered stability of pulmonary surfactant in SP-C deficient mice. *Proc Natl Acad Sci USA* 98: 6366–6371, 2001.
21. **Gopal A, Lee KYC.** Morphology and collapse transitions in binary phospholipid monolayers. *J Phys Chem B* 105: 10348–10354, 2001.
22. **Gordon LM, Lee KYC, Lipp MM, Zasadzinski JA, Walther FJ, Sherman MA, Waring AJ.** Conformational mapping of the N-terminal segment of surfactant protein B in lipid using ^{13}C-enhanced Fourier transform infrared spectroscopy. *J Peptide Res* 55: 330–347, 2000.
23. **Gupta M, Hernández-Juviel JM, Waring AJ, Bruni R, Walther FJ.** Comparison of functional efficacy of surfactant protein B analogues in lavaged rats. *Eur Respir J* 16: 1129–1133, 2000.
24. **Gupta M, Hernández-Juviel JM, Waring AJ, Walther FJ.** Function and inhibition sensitivity of the N-terminal segment of surfactant protein B (SP-B 1–25) in preterm rabbits. *Thorax* 56: 871–876, 2001.
25. **Haczku A.** Protective role of the lung collectins surfactant protein A and surfactant protein D in airway inflammation. *J Allergy Clin Immunol* 122: 861–879, 2008.
26. **Hollars CW, Dunn RC.** Submicron structure in L-α dipalmitoylphosphatidylcholine monolayers and bilayers probed with confocal, atomic force, and near-field microscopy. *Biophys J* 81: 2707–2715, 1998.
27. **Ikegami M, Whitsett JA, Martis PC, Weaver TE.** Reversibility of lung inflammation caused by SP-B deficiency. *Am J Physiol Lung Cell Mol Physiol* 289: L962–L970, 2005.
28. **Jobe AH.** Surfactant in the perinatal period. *Early Hum Dev* 29: 57–62, 1992.
29. **Johansson J, Custedt T.** Molecular structures and interactions of pulmonary surfactant components. *Eur J Biochem* 244: 675–693, 1997.
30. **Johansson J, Custedt T, Robertson B.** The proteins of the surfactant system. *Eur Respir J* 7: 372–391, 1994.
31. **Johansson E, Engvall C, Arfvidsson Lundahl P, Edwards 2005 K.** Development and initial evaluation of PEG-stabilized bilayer disks as novel model membranes. *Biophys Chem* 113: 183–192, 2005.
32. **Kageshima M, Lantz MA, Jarvis SP, Tokumoto H, Takeda S, Ptak A, Nakamura C, Miyake J.** Insight into conformational changes of a single α-helix peptide molecule through stiffness measurements. *Chem Phys Lett* 343: 77–82, 2001.
33. **Kahn MC, Anderson GJ, Anyan WR, Hall SB.** Phosphatidylcholine molecular species of calf lung surfactant. *Am J Physiol Lung Cell Mol Physiol* 269: L567–L573, 1995.
34. **Klein JM, Thompson MW, Snyder JM, George TN, Whitsett JA, Bell EF, McCray PB Jr, Nogee LM.** Transient surfactant protein B deficiency in a term infant with severe respiratory failure. *J Pediatr* 132: 244–248, 1998.
35. **Knobler CM.** Seeing phenomena in flatland: studies of monolayers by fluorescence microscopy. *Science* 249: 870–874, 1990.
36. **Kopelman AE, Mathew OP.** Common respiratory disorders of the newborn. *Pediatr Rev* 16: 209–217, 1995.
37. **Krol S, Ross M, Sieber M, Künneke S, Galla HJ, Janshoff A.** Formation of three-dimensional protein-lipid aggregates in monolayer films induced by surfactant protein B. *Biophys J* 79: 904–918, 2000.
38. **Kurutz JW, Lee KYC.** NMR structure of lung surfactant peptide SP-B11–25. *Biochemistry* 41: 9627–9636, 2002.
39. **Lee KYC, Lipp MM, Takamoto DY, Zasadzinski JA, Waring AJ.** Apparatus for the continuous monitoring of surface morphology via fluorescence microscopy during monolayer transfer to substrates. *Langmuir* 14: 2567–2572, 1998.
40. **Lipp MM, Lee KYC, Takamoto DY, Zasadzinski JA, Waring AJ.** Coexistence of buckled and flat monolayers. *Phys Rev Lett* 81: 1650–1653, 1998.
41. **Lipp MM, Lee KYC, Zasadzinski JA, Waring AJ.** Phase and morphology changes in lipid monolayers induced by SP-B protein and its amino-terminal peptide. *Science* 273: 1196–1199, 1996.
42. **McConnell HM.** Structures and transitions in lipid monolayers at the air-water interface. *Annu Rev Phys Chem* 42: 171–195, 1991.
43. **McCormack FX, Whisett JA.** The pulmonary collectins, SP-A and SP-D, orchestrate innate immunity in the lung. *J Clin Invest* 109: 707–712, 2002.
44. **Möhwald H.** Phospholipid and phospholipid-protein monolayers at the air/water interface. *Annu Rev Phys Chem* 41: 441–476, 1990.
45. **Nicholas TE, Doyle IR, Bersten AD.** Surfactant replacement therapy in ARDS: white knight or noise in the system? *Thorax* 52: 195–197, 1997.
46. **Notter RH, Wang Z, Egan EA, Holm BA.** Component-specific surface and physiological activity in bovine-derived lung surfactants. *Chem Phys Lipids* 114: 21–34, 2002.
47. **Patthy L.** Homology of the precursor of pulmonary surfactant-associated protein SP-B with prosaposin and sulfated glycoprotein 1. *J Biol Chem* 266: 6035–6037, 1991.
48. **Pison U, Herold R, Schürch S.** The pulmonary surfactant system: biological functions, components, physiological properties and alterations during lung disease. *Colloids Surfaces* 114: 165–184, 1996.
49. **Pocivavsek L, Dellsy R, Kern A, Johnson S, Lin B, Lee KYC, Cerda E.** Stress and fold localization in thin elastic membranes. *Science* 320: 912–916, 2008.
50. **Pocivavsk L, Frey SL, Krishan K, Gavrilov K, Ruchala P, Waring AJ, Walther FJ, Dennin M, Witten TA, Lee KYC.** Lateral stress relaxation and collapse in lipid monolayers. *Soft Matt* 4: 1–12, 2008.
51. **Robertson B, Halliday HL.** Principle of surfactant replacement. *Biochim Biophys Acta* 1408: 346–361, 1998.
52. **Sanders CR, Prosser RS.** Bicelles: a model membrane system for all seasons? *Structure* 6: 1227–1234, 1998.

53. **Sarker M, Waring AJ, Walther FJ, Keough KMW, Booth V.** Structure of mini-B, a functional fragment of surfactant protein B, in detergent micelles. *Biochemistry* 46: 11047–11056, 2007.
54. **Schürch S, Goerke J, Clements JA.** Direct determination of surface tension in the lung. *Proc Natl Acad Sci USA* 73: 4698–4702, 1976.
55. **Seeger W, Gunther A, Walmrath HD, Grimminger F, Lasch HG.** Alveolar surfactant and adult respiratory distress syndrome. Pathogenic role and therapeutic prospects. *Clin Invest* 71: 177–190, 1993.
56. **Serrano AG, Pérez-Gil J.** Protein-lipid interactions and surface activity in the pulmonary surfactant system. *Chem Phys Lipids* 141: 105–118, 2006.
57. **Serrano AG, Ryan M, Weaver TE, Pérez-Gil J.** Critical structure-function determinants within the N-terminal region of pulmonary surfactant protein SP-B. *Biophys J* 90: 238–249, 2006.
58. **Seurynck-Servoss SL, Dohm MT, Barron AE.** Effects of including an N-terminal insertion region and arginine-mimetic side chains in helical peptoid analogues of lung surfactant protein B. *Biochemistry* 45: 11809–11818, 2006.
59. **Shanmukh S, Biswas N, Waring AJ, Walther FJ, Wang Z, Chang Y, Notter RH, Dluhy RA.** Structure and properties of phospholipid-peptide monolayers containing monomeric SP-B 1–25 II. Peptide confirmation by infrared spectroscopy. *Biophys Chem* 113: 233–244, 2005.
60. **Shannon DC, Bunnell JB.** Dipalmitoyl lecithin aerosol in RDS. *Pediatr Res* 10: 997, 1976.
61. **Stocks J, Quanjer PH.** Reference values for residual volume, functional residual capacity, and total lung capacity. *Eur Respir J* 8: 492–506, 1995.
62. **Sutinen S, Riska H, Backman R, Sutinen SH, Roseth B.** Alveolar lavage fluid (ALF) of normal volunteer subjects: cytologic, immunocytochemical, and biochemical reference values. *Resp Med* 89: 85–92, 1995.
63. **Takamoto DY, Lipp MM, von Nahmen A, Lee KYC, Waring AJ, Zasadzinski JA.** Interaction of lung surfactant proteins with anionic phospholipids. *Biophys J* 81: 153–169, 2001.
64. **Tokieda K, Whitsett JA, Clark JC, Weaver TE, Ikeda K, McConnell KB, Jobe AH, Ikegami M, Iwamoto HS.** Pulmonary dysfunction in neonatal SP-B-deficient mice. *Am J Physiol Lung Cell Mol Physiol* 273: L875–L882, 1997.
65. **Triba MN, Warschawski DE, Devaux PF.** Reinvestigation by phosphorus NMR of lipid distribution in bicelles. *Biophys J* 88: 1887–1901, 2005.
66. **Vandenbussche G, Clercx A, Clercx M, Curstedt T, Johansson J, Jornvall H, Ruysschaert JM.** Secondary structure and orientation of the surfactant protein SP-B in a lipid environment—a fourier-transform infrared-spectroscopy study. *Biochemistry* 31: 9169–9176, 1992.
67. **Veldhuizen EJA, Waring AJ, Walther FJ, Batenburg JJ, van Golde LMG, Haagsman HP.** Dimeric N-terminal segment of human surfactant protein B (sSP-B 1–25) has enhanced surface properties compared to monomeric SP-B 1–25. *Biophys J* 79: 377–384, 2000.
68. **Vold RR, Prosser RS.** Magnetically oriented phospholipid bilayered micelles for structural studies of polypeptides: does the ideal bicelle exist? *J Magn Reson* 113: 267–271, 1996.
69. **Walther FJ, Hernández-Juviel JM, Gordon LM, Sherman MA, Waring AJ.** Dimeric surfactant protein B peptide SP-B 1–25 in neonatal and acute respiratory distress syndrome. *Exp Lung Res* 28: 623–640, 2002.
70. **Walther FJ, Hernández-Juviel JM, Mercado PE, Gordon LM, Waring AJ.** Surfactant with SP-B and SP-C analogues improves lung function in surfactant-deficient rats. *Bio Neonate* 82: 181–187, 2002.
71. **Waring AJ, Walther FJ, Gordon LM, Hernandez-Juviel JM, Hong T, Sherman MA, Alonso C, Alig T, Braun A, Bacon D, Zasadzinski JA.** The role of charged amphipathic helices in the structure and function of surfactant protein B (SP-B). *J Peptide Res* 66: 364–374, 2005.
72. **Wang Y, Rao KMK, Demchuk E.** Topographical organization of the N-terminal segment of lung pulmonary surfactant protein B (SP-B 1–25) in phospholipid bilayers. *Biochemistry* 42: 4015–4027, 2003.
73. **Wu GH, Majewski J, Ege C, Kjaer K, Weygand MJ, Lee KYC.** Interaction between lipid monolayers and poloxamer 188: An X-ray reflectivity and diffraction study. *Biophys J* 89: 3159–3173, 2005.

73a. **Zelig D, Haber S.** Hydrodynamic cleansing of pulmonary alveoli. *SIAM J Appl Math* 63: 195–201, 2002.